# Effect of synthesis parameters on the performance of alkali-activated Non-conformant EN 450 Pulverised Fuel Ash

**S. Adu-Amankwah, J.M. Khatib, D.E. Searle, L. Black**

## Abstract

The fly ash reported in this paper is coarser than conventional PFA, with loss on ignition (LOI) exceeding 10.8%. Consequently, it is precluded from being used as a supplementary cementitious material (SCM) according to EN 450 and disposed in landfills. Alkali-activation of such PFAs is considered here. Three concentrations of sodium hydroxide (NaOH) were separately blended with water glass at different ratios to modify the silica modulus. Heat of reaction, setting time, compressive strength and drying shrinkage were investigated as a function of activator composition. Specimens were either cured at room temperature or hydro-thermally treated at 75°C for five hours. The results show that by optimizing the activator composition, a binder with a 28 day compressive strength of 25MPa can be synthesised from such PFAs even at room temperature. Among the activator parameters, the alkali content was observed to be most influential.

*Keywords: Geopolymer, fly ash, loss on ignition, shrinkage, setting time, EN 450*

## 1.0 Introduction

Alkali-activated binders present a low-carbon alternative to Portland cement [1]. This class of binders are obtained from the reaction between alumina-silicate feedstock and concentrated solutions of alkali hydroxides [2, 3], silicates [4], sulphates [5], carbonates [6] or combinations thereof [7, 8]. An overview of the mechanism responsible for the transformation of the initial constituent materials into a binder has been extensively reported [9, 10]. At higher pH, reactive alumina and silicates dissolve from the feedstock and when speciation equilibrium conditions are attained, the species precipitate into gels. Progressive interconnectivity of precipitated species, reorganization and condensation lead to a solid binder phase.

The parameters which influence the fresh and hardened properties of alkali-activated binders fall into two categories. That is, those inherent within the constituent materials, and the externally applied conditions. With regards to the intrinsic parameters, a variety of activators have been studied [11-14], as have a variety of feedstock materials [13-15]. The proportioning of these materials are system specific [16, 17] and consequently determine the properties of the binder produced [3]. The effect of silica moduli [4, 18, 19], silicate to alumina [20-22] and water to silicate ratios have all been explored. However, mechanical performance is usually related to the silica modulus [23, 24]. Recent studies have suggested that the amorphous silica to alumina ratio ($SiO_2/Al_2O_3$) also plays a significant role on the early age properties [25]. The optimum $SiO_2/Al_2O_3$ ratio however depends on the calcium content of the feedstock [26]. It therefore follows that a generalised mix formulation in these binders does not exist, thus necessitating the need to optimize the activator composition for every feedstock.

A range of alumina-silicate source materials for the synthesis of this class of binders have been explored in the literature [27-30]. Most of the explored feedstock however requires thermal or mechanical processing in order to obtain reasonable performance [31-36]. As a result, pulverised fuel ash (PFA), an industrial by-product which can be used directly will remain a popular and rather cheaper option. By virtue of being an industrial waste, the properties of PFA are dependent on coal source [25], pulverisation and combustion conditions [37, 38] which are often tailored to maximize energy output rather than the quality of the ash. Technology and control of environmental pollution also dictates the ash collection method which also impacts on the quality of the PFA [39]. This leads to wide compositional variability, even from a single power stations [40, 41].

The variability of PFAs even from the same source restricts the use of some PFAs as SCMs. For example, the European norm EN 450-1 imposes compositional and physical requirements for PFA as SCMs; unburnt carbon content below 9%, as well as a maximum content of 40% coarser than 45 microns [42]. These non-conformant PFAs end up as landfill wastes at a cost to power generators. Previously reported alkali-activated PFAs offer potential technical advantages. However, the PFA feedstock mostly conforms to the EN 450 criteria [3, 43-47] thus competing with those used as SCMs in composite cements. The suitability of Non conformant PFA for geopolymer synthesis has not been studied previously and constitutes the objective of this paper.

## 2.0 Experimental Details

### 2.1 Materials

Unconditioned PFA obtained directly from electrostatic precipitating hubs from a UK Power station was used for this study. The XRF composition and the particle size distribution obtained through Malvern Mastersizer are shown in Table 1 and Figure 1 respectively.

Table 1 XRF composition of the PFA under investigation

| Oxide | $SiO_2$ | $Al_2O_3$ | Fe2O | CaO | MgO | $Na_2O$ | $K_2O$ | $TiO_2$ | $SO_2$ | LOI |
|---|---|---|---|---|---|---|---|---|---|---|
| % | 51.42 | 24.33 | 13.10 | 4.06 | 2.16 | 0.85 | 2.45 | 1.15 | 0.52 | 10.78 |

Iso-propanol was used as dispersant for the PSD measurement and the Fraunhofer method was implemented for data evaluation. The LOI was separately determined according to the method in EN 196-2 hence the sum of the oxide compositions including the LOI exceeding 100%.

Activators for the study were formulated from water glass solution and laboratory grade sodium hydroxide pellets (98% purity). The water glass solution composed of

8.5±0.3 % $Na_2O$ and 27.8±0.5% $SiO_2$. The viscosity and specific gravity were 70-120MPa.s and 1.385g/cm$^3$ respectively. Three concentrations of sodium hydroxide solutions (8, 15 and 20M) were added at different levels to modify the silica modulus [4]. The activator composition and calculated molar ratios are shown in Table 2. The choice of the investigated activator composition range was based on the varied optimal ranges reported in the literature [48].

## 2.2 Sample preparation and testing

Isothermal conduction calorimetry was conducted on an 8-channel TAM Air calorimeter. 6.0g of PFA and 3.0g of the activating solutions were weighed and kept in the calorimeter until a stable baseline was attained. The activating solution was subsequently injected and then mixed in situ.

Setting time was measured on paste samples according to BS EN 196-3 using the Vicat apparatus. The entire test setup was submerged under water as prescribed in the norm. The reported setting times are average of three measurements. Mixing procedure for setting time, shrinkage and compressive strength testing were based on the recommendations of BS EN 196-1. The activating solution to feedstock ratio was maintained at 0.5. This was established from the consistency tests during the scoping studies.

Compressive strength and drying shrinkage were measured on mortar samples in replicates of three. The mortar specimens were prepared with 1:1:0.5 PFA/sand/activator ratios. The mix ratio was adopted in order to maintain the activating solution/PFA ratio at the same level as that which was used for the setting time measurement. The strength test specimens were 50mm cubes while shrinkage was assessed from demountable mechanical (demec) points fitted to 40x40x160mm prisms after either 1 day curing at room temperature or hydrothermal curing at 75°C. Autogenous shrinkage was taken as the shrinkage on samples sealed with flash band and monitored from 1 day. Two curing regimes were assessed; continuous curing at room temperature and hydro-thermally treated at 75°C for five hours, as performed elsewhere [49]. The latter was achieved by introducing the moulds in a pan which was half-filled with water and covered with an aluminium foil.

Table 2 Activator composition and computed parameters

| Designation | A | B | C | D | E | F | G | H | J | K | L | M | N | P | Q |
|---|---|---|---|---|---|---|---|---|---|---|---|---|---|---|---|
| NaOH conc | Group1 waterglass/8M | | | | | Group2 waterglass/15M | | | | | Group3 waterglass/20M | | | | |
| $SiO_2/Na_2O$ | 0.5 | 1.1 | 1.7 | 2.6 | 3.1 | 0.4 | 0.8 | 1.4 | 2.3 | 3.0 | 0.3 | 0.7 | 1.2 | 2.2 | 2.9 |
| Molar $H_2O$ | 5.4 | 5.2 | 5.0 | 4.9 | 7.5 | 4.7 | 4.7 | 4.8 | 4.8 | 7.4 | 4.4 | 4.5 | 4.6 | 4.7 | 6.3 |
| $H_2O/Na_2O$ | 21 | 23 | 27 | 31 | 52 | 12 | 16 | 20 | 26 | 50 | 10 | 13 | 17 | 25 | 41 |

| | | | | | | | | | | | | | | | |
|---|---|---|---|---|---|---|---|---|---|---|---|---|---|---|---|
| $H_2O/SiO_2$ | 39 | 23 | 16 | 12 | 17 | 34 | 20 | 15 | 12 | 17 | 31 | 19 | 14 | 11 | 14 |
| w/solids | 0.3 | 0.3 | 0.3 | 0.2 | 0.4 | 0.2 | 0.2 | 0.2 | 0.2 | 0.4 | 0.2 | 0.2 | 0.2 | 0.2 | 0.3 |

Note:  Entries rounded to 1 decimal place.

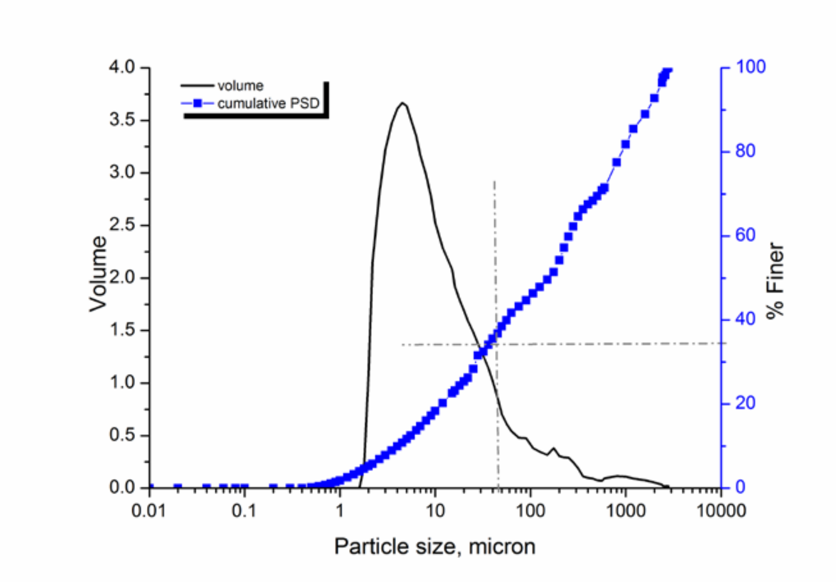


Figure 1 Particle size distribution of the PFA under investigation

## 3.0 Results and discussion

### 3.1 Reaction kinetics

The objective here is to clarify the influence of alkali concentration and dosage on the reactivity and kinetics.  The data presented here is limited to 20˚C because it was not possible to perform hydrothermal curing in a calorimeter.  Additionally, the effect of temperature has already been clarified elsewhere [3, 50, 51].

The kinetics of early stage reactions as a function of activator composition are shown in Figures 2 (a-c).  In all formulations, the heat flow was characterized by a single exothermic peak which occurred within 20 minutes after mixing.  A short induction stage can be seen in the 8M NaOH mixes (Figure 2a); but no appreciable induction was observed in the 15M and 20M mixes.

At a given NaOH molarity, an inverse relationship was noticed between the silicate dosage and the rate of reaction.  This effect was less distinct in the 8M NaOH mixes except at silica moduli of 2.6 and 3.1.  Comparison between Figures 2a and 2b depicts the significance of the alkali concentration which was used to modify the silica modulus of water glass.  The rate of reaction was accelerated with increasing alkali concentration.  However, this seems to reach a maximum at 15M NaOH. Beyond this, differences between 15 and 20M NaOH were not visible.

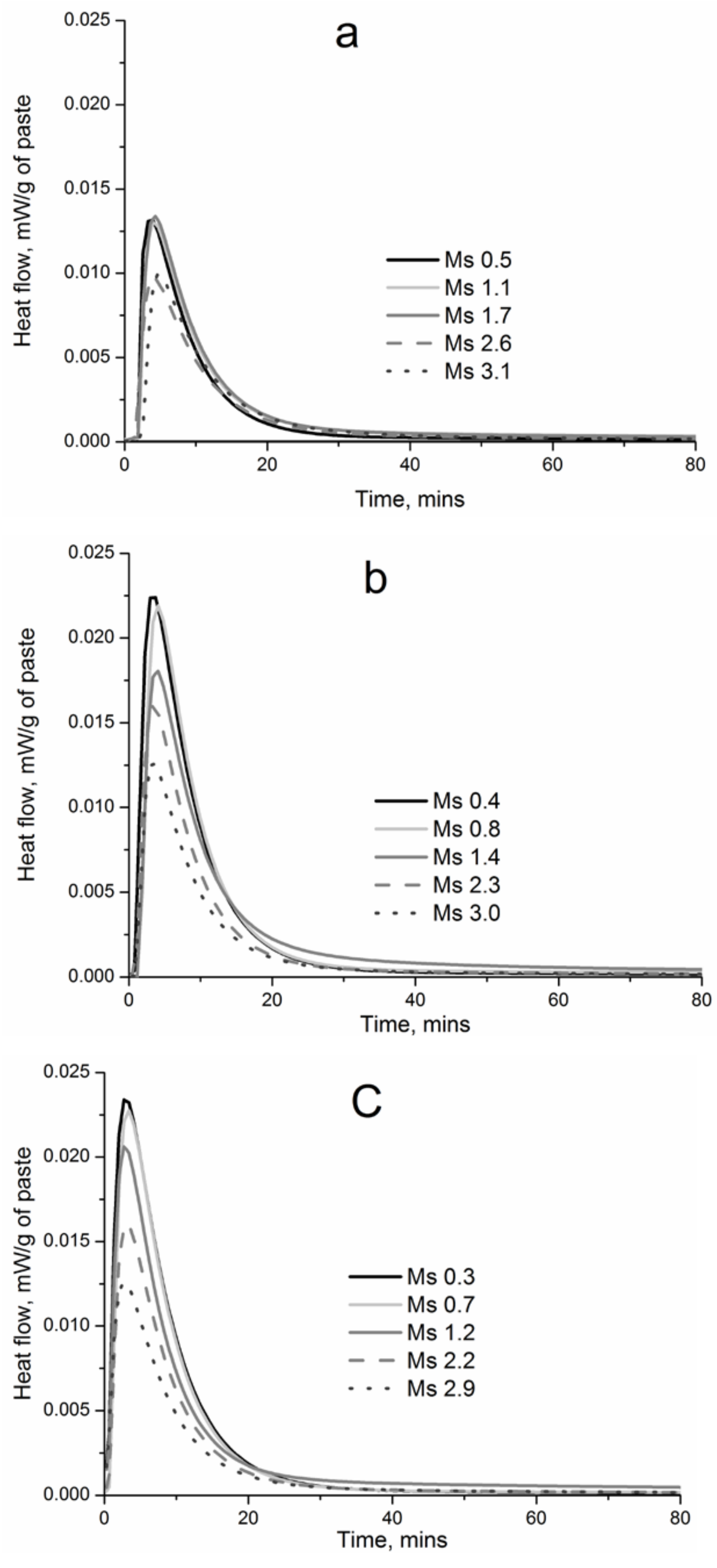
a
b
C
Heat flow, mW/g of paste
Time, mins
0.025
0.020
0.015
0.010
0.005
0.000
0
20
40
60
80
Ms 0.5
Ms 1.1
Ms 1.7
Ms 2.6
Ms 3.1
Ms 0.4
Ms 0.8
Ms 1.4
Ms 2.3
Ms 3.0
Ms 0.3
Ms 0.7
Ms 1.2
Ms 2.2
Ms 2.9

Figure 2 Effect of alkali concentration and activator composition on the heat flow of alkali-activated RoS PFA: (a) 8M NaOH blends; (b) 15M NaOH blends; (c) 20M NaOH blends. Refer to Table 2 for designations

In the synthesis of alkali-activated binders, the activator is often specified in terms of the silica moduli [24, 43, 52]. The general trend of improved rate of reaction with decreasing silica modulus is consistent with the literature [24]. However, the heat flow data presented above have shown that, slight modifications in the silica modulus can influence the reaction kinetics significantly. The mechanisms underlying these observations seem to relate to the molarity of the alkali solution rather than the silica modulus. The heat flow data is consistent with the previously espoused geopolymerisation mechanism [9, 43]. The dissolution, polymerization and condensation processes are coupled. However, dissolution is exothermic and accounts for the single heat flow peak. Subsequent reactions seem to produce minimal net heat of reaction after the first 40minutes of mixing. The maximum heat evolved for each of the three groups was plotted against the silica modulus and shown in Figure 3. The trends are similar irrespective of the alkali concentration. The maximum heat decreased with increasing silica modulus. At any given moduli, the maximum heat was similar at 15 and 20M but lower at 8M.

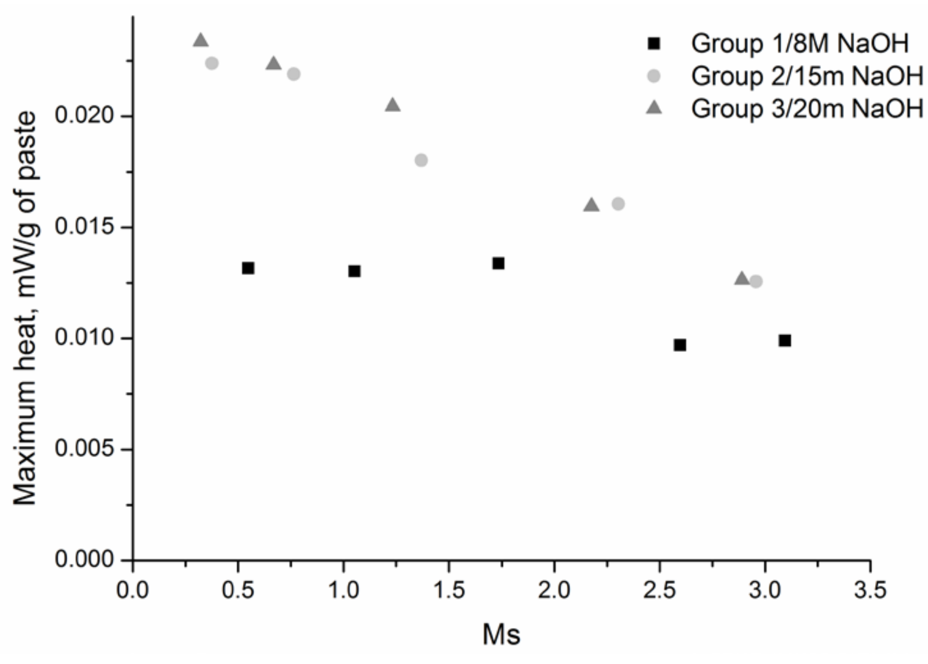


Figure 3 Effect of the silica modulus on the maximum heat evolved in activated RoS PFA

At a given molarity, increasing the dosage of the original waterglass solution reduces alkalis and the hydroxyl content. Consequently dissolution of aluminate and silicate species from the precursor is restricted. Regarding polymerisation, excess reactive silicates in the reacting matrix has been reported to promote poly-sialate-siloxo/disiloxo type geopolymers [53, 54]. The silicate-silicate reaction is slower compared to silicate-aluminate; however, because the overall dissolved species is lower at high silica moduli, polymerisation is retarded.

## 3.2 Setting time

Final setting times of the investigated mixes as a function of activator composition and total w/solid ratios are presented in Figures 4 (a-d). Setting time, which is indicative of precipitation of network forming products, is strongly influenced by the composition of the activating solution. The strongest correlation was observed with the silica moduli and the water to alkali ratios while the worst was observed from the water to silica ratio. According to the data, increasing the silica moduli or the water to alkali ratio of the activating solution delayed setting. The accelerating effect of higher alkali concentration on the rate of reaction and consequently quicker setting has been reported elsewhere [55]. Flash setting was observed in the mixes with $SiO_2/Na_2O$ below one. The overall water deficiency at these moduli ($SiO_2/Na_2O$ <1) (see Fig 2-d) potentially resulted in accelerated gelation arising from the pairing of dissolved ionic species in close proximity which then leads to rapid setting. Final setting time was over 6 hours at silica modulus of approximately 3. This may also be attributed to the lower alkali content retarding the dissolution from the feedstock [24, 56].

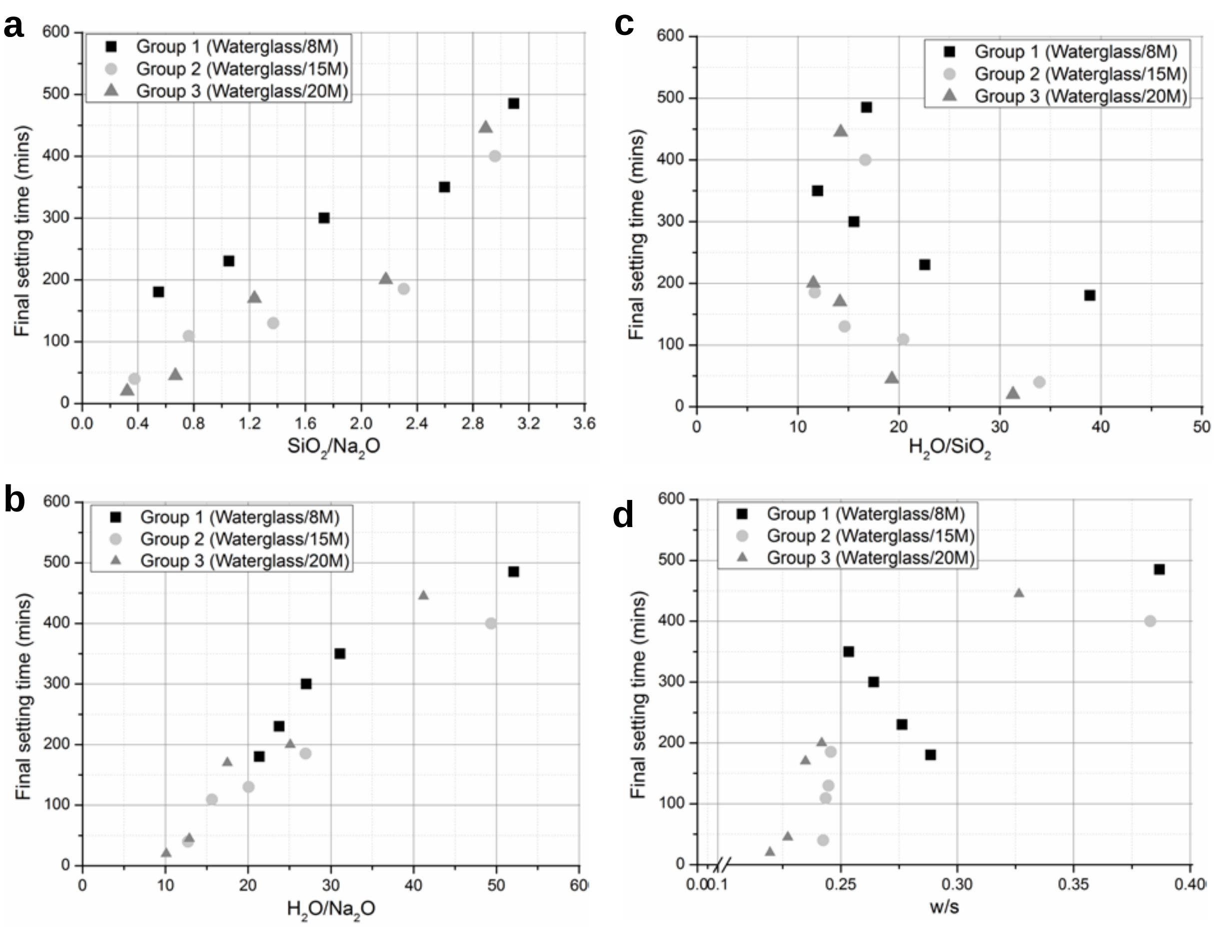

Figure 4 Initial times of RoS PFA as function of activator parameters: Effect of (a) silica modulus; (b) molar water/ alkali (c) molar water/ silica (d) water/solid ratios

Moreover, at higher silica moduli, the expected microstructure would evolve from silicate-silicate polymers. This however takes place at a slower rate compared to silicate-alumina [54]. The setting times agree with the heat of reaction data presented in Figure 2 and are consistent with the trends reported in [24]. Despite the importance of alkalis to silicate dissolution, it is worth noting that excess alkalis in solution can also impede the reaction [57].

### 3.3 Compressive strength evolution

Table 3 shows the effects of curing regime and activator composition on compressive strength after 1 and 28 days. Alongside compressive strength, the cumulative heat after 1 day is presented for each group. The impact of hydro-thermal curing on early age strength development was obvious. Compressive strength was higher following hydrothermal treatment compared to room temperature curing. The magnitude of compressive strength however depended strongly on the activator composition.

Table 3 Effects of silica modulus (Ms) and $H_2O/Na_2O$ on compressive strength following curing at room temperature and hydrothermal curing at 75°C.

| Mix ID | Ms | $H_2O/Na_2O$ | Compressive strength, MPa @ 20°C | | Compressive strength, MPa, Hydrothermal @75°C | | Cum. Heat @ 1D, J/g of paste |
|---|---|---|---|---|---|---|---|
| | | | 1D | 28D | 1D | 28D | |
| A | 0.54 | 21.37 | 1.43 | 4.80 | 2.91 | 11.67 | 13.48 |
| B | 1.05 | 23.77 | 5.63 | 14.83 | 16.31 | 23.24 | 15.36 |
| C | 1.74 | 27.02 | 7.10 | 12.59 | 10.82 | 20.33 | 16.60 |
| D | 2.60 | 31.12 | 3.75 | 5.74 | 4.67 | 6.00 | 9.58 |
| E | 3.09 | 52.10 | 1.35 | 2.55 | 2.10 | 5.72 | 9.75 |
| F | 0.38 | 12.61 | 1.70 | 11.03 | 3.24 | 12.79 | 19.73 |
| G | 0.76 | 15.62 | 5.90 | 16.24 | 12.99 | 18.68 | 21.24 |
| H | 1.37 | 20.07 | 11.39 | 25.53 | 19.49 | 35.65 | 32.91 |
| J | 2.30 | 26.94 | 3.79 | 9.59 | 4.26 | 14.92 | 13.52 |
| K | 2.96 | 49.38 | 1.81 | 2.10 | 1.25 | 3.73 | 10.50 |
| L | 0.32 | 10.11 | 2.65 | 7.17 | 5.84 | 13.11 | 19.01 |
| M | 0.67 | 12.91 | 4.34 | 14.13 | 6.31 | 15.68 | 23.49 |
| N | 1.23 | 17.49 | 8.12 | 17.30 | 17.10 | 29.10 | 42.98 |

| | | | | | | | |
|---|---|---|---|---|---|---|---|
| P | 2.18 | 25.11 | 4.54 | 13.77 | 4.20 | 14.26 | 12.75 |
| Q | 2.89 | 41.19 | 1.01 | 1.74 | 1.21 | 3.04 | 10.88 |

Note: The standard deviation the data points in the table ranged between 0.3 to 0.7MPa.

In the samples cured at room temperature, strength was lowest in the samples in which were activated the 8M NaOH blended solutions. Modifying the silica modulus with 20M NaOH did not necessarily improve strength. Slightly lower strength was observed on the 20M NaOH samples which were cured at room temperature. With respect to the silica modulus, it is apparent that, irrespective of curing regime and molarity of sodium hydroxide, an optimum existed. The highest compressive strength was obtained from the moduli range 1.2 – 1.7 and water/alkali ratio of 20. The latter depends more on the alkali content than the initial water or silicate content.

These are consistent with the literature [3, 58]. Provided the mix is workable, the water content is not an important parameter [3]. Plausible reason is the reaction mechanism [9] in these binders. Here, water which is consumed in the dissolution process reforms during gelation and rearrangement; silicates on the other hand only play a transitional role in the polymerization process [3, 4]. The silicates play a vital role only when dissolution of species from the feedstock is underway. The dissolved silicates in the activator then potentially act as nucleation sites for growth of polymeric chains similar to the effect of seeding on C-S-H evolution in conventional clinker based systems [59].

As noticed from the heat flow data above (see Figure 2), the alkali content strongly influences the kinetics of reaction in these binders and consequently the compressive strength. A threshold alkali concentration relative to dissolved aluminates has however been reported elsewhere [55]. Silica modulus below 1.0 presents highly alkaline systems which leads to rapid super-saturation of dissolved species. This was also manifested in the setting times (Figure 4a). The excess silicates lead to coagulation of the activating solution which inhibits dissolution and subsequent polymerization.

### 3.4 Drying shrinkage

Figure 4 shows typical total shrinkage and shrinkage due to progressive reactions (measurement commencing after 1 day and subsequently referred to as autogenous shrinkage) for the two curing regimes investigated for the PFA activated with Ms 0.8/15M. The data shows that the curing regime strongly influences drying and autogenous shrinkage. As would be expected, water is evaporated during the hydrothermal curing. The shrinkage associated with the latter was however not taken into consideration. Following the hydrothermal curing, the sample has less water and better developed microstructure. Conversely, the room temperature cured samples reacted slowly with more water available to be removed by drying. The trend between the two curing regimes was consistent irrespective of the activator composition. This implies that, reaction persists in the room temperature cured specimens over the test duration while that of the hydrothermally cured samples were marginal. Higher drying shrinkage in the samples cured at room temperature was expected due to slower rate of reaction and availability of moisture to dissolve $CO_2$, thus amplifying shrinkage due to carbonation; and also evaporation of water.

The effects of activator composition on the net drying shrinkage of the investigated mixes are shown in Figure 5. The trends were similar in the hydrothermally cured samples hence not duplicated. The results show higher shrinkage with increasing silica moduli irrespective of the NaOH concentration used to modify the activating solution. The magnitude of drying shrinkage however showed strong dependence on the alkali concentration. For example, slight changes in the modulus resulting from using 15M rather than 8M NaOH doubled the drying shrinkage magnitude. However, for approximately similar modulus, the 20M NaOH showed lesser shrinkage compared to the 15M blends. In summary, highest drying shrinkage was noticed when the activator modulus was modified with 15M NaOH and lowest at the 8M NaOH.

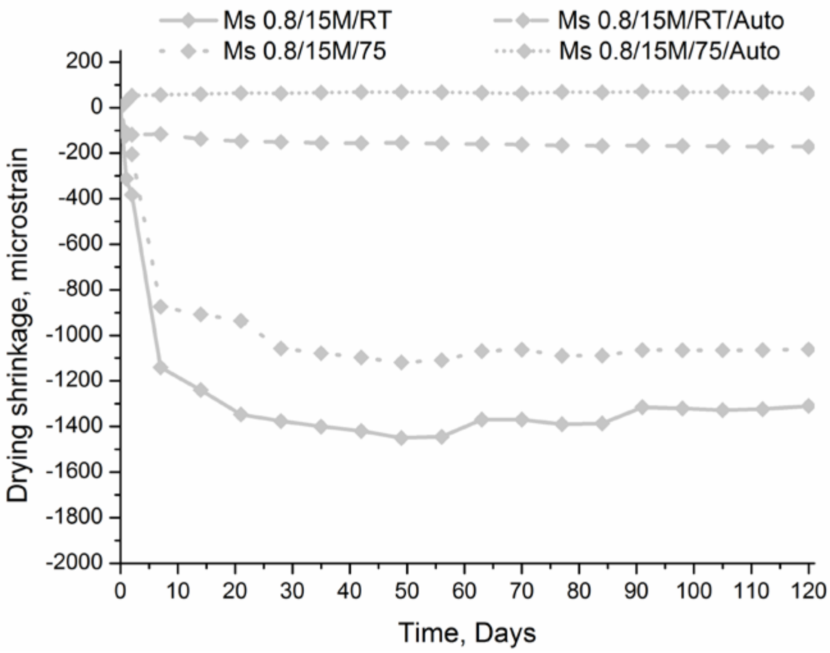


Figure 4 Effect of curing temperature on drying and autogenous shrinkage of activated RoS PFA

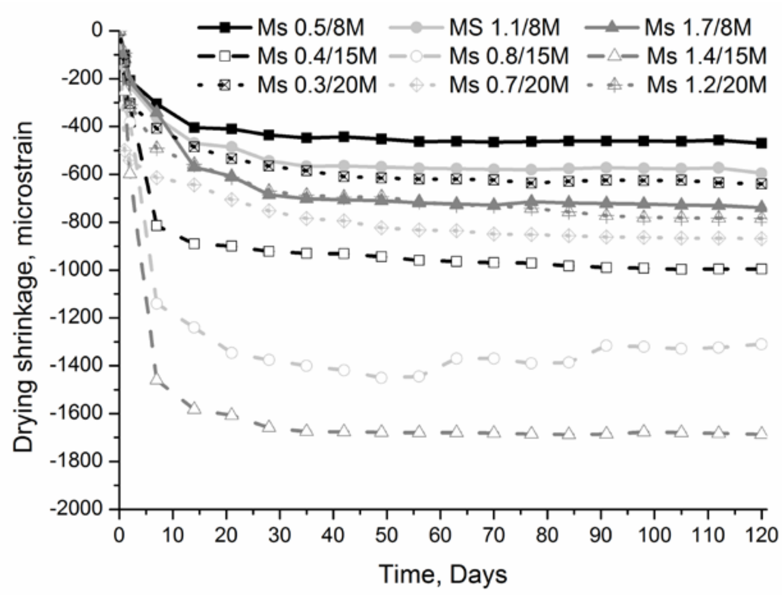


Figure 5 Effect of activator composition on the drying shrinkage of room temperature cured specimens. Solid lines: 8M NaOH; dash lines: 15M NaOH; dots= 20M NaOH blends

The observations seem to relate closely to the moisture in the specimen [60]. Considering that the water to alkali ratio increased with increasing silica modulus, higher proportion of water would be available to evaporate at high silica modulus. With regards to alkali concentration, increasing the molarity implied higher solute to water ratio as shown in Table 2; however the shrinkage did not follow this trend. The observations can be attributed to the extent of reaction in the mixes. Given that the hydrolysis of alumina-silicates consumes water but water reforms during condensation [9, 12], higher shrinkage was expected in the samples with greater reaction. This is also consistent with the compressive strength data presented above.

## 4.0 Conclusions

The effect of activator composition on the reaction kinetics and performance of activated high LOI PFA have been investigated. It has been shown that, by optimizing the activating solution, a binder with up to 25MPa can be produced from EN 450 non-conformant PFA at room temperature. Drying shrinkage was considerably higher than conventional cements. Regarding the activating solution parameters, the silica moduli and water/alkali ratios significantly influenced reaction kinetics, setting time, strength and dimensional stability. Reactivity improved with increasing alkali concentration but decreased at high silicate content of the activating solution. Alkali activation therefore offers the possibility of making good use PFAs which would otherwise be disposed in landfills at a cost and attendant environmental problems.

## Acknowledgement

The author is thankful to the University of Wolverhampton who funded this project.

## References

[1] J.L. Provis, A. Palomo, C. Shi, Advances in understanding alkali-activated materials, Cement and Concrete Research, 78, Part A (2015) 110-125.

[2] A. Palomo, S. Alonso, A. Fernandez-Jimenez, Alkaline Activation of Fly Ashes: NMR Study of the Reaction Products, J Am Ceram Soc, 87 (2004) 1141-1145.

[3] A. Palomo, M.W. Grutzeck, M.T. Blanco, Alkali-activated fly ashes: A cement for the future, Cement and Concrete Research, 29 (1999) 1323-1329.

[4] M. Criado, A. Fernández-Jiménez, A. Palomo, I. Sobrados, J. Sanz, Effect of the SiO2/Na2O ratio on the alkali activation of fly ash. Part II: 29Si MAS-NMR Survey, Microporous and Mesoporous Materials, 109 (2008) 525-534.

[5] A.M. Rashad, Y. Bai, P.A.M. Basheer, N.C. Collier, N.B. Milestone, Chemical and mechanical stability of sodium sulfate activated slag after exposure to elevated temperature, Cement and Concrete Research, 42 (2012) 333-343.

[6] S. Bernal, J. Provis, R. Myers, R. San Nicolas, J.J. van Deventer, Role of carbonates in the chemical evolution of sodium carbonate-activated slag binders, Mater Struct, 48 (2015) 517-529.

[7] L. Verdolotti, S. Iannace, M. Lavorgna, R. Lamanna, Geopolymerization reaction to consolidate incoherent pozzolanic soil, J Mater Sci, 43 (2008) 865-873.

[8] G. Zheng, X. Cui, W. Zhang, Z. Tong, Preparation of geopolymer precursors by sol–gel method and their characterization, J Mater Sci, 44 (2009) 3991-3996.

[9] P. Duxson, A. Fernández-Jiménez, J.L. Provis, G.C. Lukey, A. Palomo, J.S.J. van Deventer, Geopolymer technology: the current state of the art, Journal of Materials Science, 42 (2007) 2917-2933.

[10] J.L. Provis, Geopolymers: Structures, Processing, Properties and Industrial Applications, in: J.S.J.v.D. J L Provis (Ed.) Geopolymers: Structures, Processing, Properties and Industrial Applications, Woodhead Publishing Materials, 2009, pp. 37-66.

[11] J. Davidovits, Geopolymers and geopolymeric materials, Journal of Thermal Analysis, 35 (1989) 429-441.

[12] A. Fernández-Jiménez, A. Palomo, M. Criado, Microstructure development of alkali-activated fly ash cement: a descriptive model, Cement and Concrete Research, 35 (2005) 1204-1209.

[13] C.K. Yip, G.C. Lukey, J.S.J. van Deventer, The coexistence of geopolymeric gel and calcium silicate hydrate at the early stage of alkaline activation, Cement and Concrete Research, 35 (2005) 1688-1697.

[14] P. Duxson, J.L. Provis, G.C. Lukey, S.W. Mallicoat, W.M. Kriven, J.S.J. van Deventer, Understanding the relationship between geopolymer composition, microstructure and mechanical properties, Colloids and Surfaces A: Physicochemical and Engineering Aspects, 269 (2005) 47-58.

[15] Z. Zhang, J.L. Provis, A. Reid, H. Wang, Mechanical, thermal insulation, thermal resistance and acoustic absorption properties of geopolymer foam concrete, Cement and Concrete Composites, 62 (2015) 97-105.

[16] Y. Chen, F. Han, L. Wu, Leaching of Lead from Geopolymer Prepared by Waste Acid Residue, Procedia Engineering, 102 (2015) 395-398.

[17] M. Izquierdo, X. Querol, J. Davidovits, D. Antenucci, H. Nugteren, C. Fernández-Pereira, Coal fly ash-slag-based geopolymers: Microstructure and metal leaching, Journal of Hazardous Materials, 166 (2009) 561-566.

[18] A.S. de Vargas, D.C.C. Dal Molin, A.C.F. Vilela, F.J.d. Silva, B. Pavão, H. Veit, The effects of Na2O/SiO2 molar ratio, curing temperature and age on compressive strength, morphology and microstructure of alkali-activated fly ash-based geopolymers, Cement and Concrete Composites, 33 (2011) 653-660.

[19] S.A. Bernal, R.M. de Gutierrez, J.L. Provis, V. Rose, Effect of silicate modulus and metakaolin incorporation on the carbonation of alkali silicate-activated slags, Cement and Concrete Research, 40 (2010) 898-907.

[20] C. Tennakoon, P.D. Silva, K. Sagoe-Crentsil, J.G. Sanjayan, Influence and role of feedstock Si and Al content in Geopolymer synthesis, Journal of Sustainable Cement-Based Materials, 4 (2015) 129-139.

[21] A. Hajimohammadi, J.L. Provis, J.S.J.v. Deventer, One-Part Geopolymer Mixes from Geothermal Silica and Sodium Aluminate, Ind Eng Chem Res, 47 (2008) 9396-9405.

[22] A. Fernández-Jiménez, A. Palomo, I. Sobrados, J. Sanz, The role played by the reactive alumina content in the alkaline activation of fly ashes, Microporous and Mesoporous Materials, 91 (2006) 111-119.

[23] A. Fernandez-Jimenez, I. García-Lodeiro, A. Palomo, Durability of alkali-activated fly ash cementitious materials, J Mater Sci, 42 (2007) 3055-3065.

[24] S.A. Bernal, J.L. Provis, V. Rose, R. Mejía de Gutierrez, Evolution of binder structure in sodium silicate-activated slag-metakaolin blends, Cement and Concrete Composites, 33 (2011) 46-54.

[25] M. Ahmaruzzaman, V.K. Gupta, Application of Coal Fly Ash in Air Quality Management, Ind Eng Chem Res, 51 (2012) 15299-15314.

[26] K. Sagoe-Crentsil, P.D. Silva, Alkali-Activated Binders: Early age nucleation reactions, chemical phase evolution and their implications on system properties, J Chin Ceram Soc, 43 (2015) 1449-1457.

[27] J.G.S. van Jaarsveld, J.S.J. van Deventer, G.C. Lukey, The effect of composition and temperature on the properties of fly ash- and kaolinite-based geopolymers, Chemical Engineering Journal, 89 (2002) 63-73.

[28] R.R. Lloyd, J.L. Provis, J.S.J. van Deventer, Pore solution composition and alkali diffusion in inorganic polymer cement, Cement and Concrete Research, 40 (2010) 1386-1392.

[29] G. Zheng, X. Cui, D. Huang, J. Pang, G. Mo, S. Yu, Z. Tong, Alkali-activation reactivity of chemosynthetic Al2O3–2SiO2 powders and their 27Al and 29Si magic-angle spinning nuclear magnetic resonance spectra, Particuology, 22 (2015) 151-156.

[30] K.-t. Wang, Y. He, X.-l. Song, X.-m. Cui, Effects of the metakaolin-based geopolymer on high-temperature performances of geopolymer/PVC composite materials, Applied Clay Science, 114 (2015) 586-592.

[31] C. Ruiz-Santaquiteria, A. Fernández-Jiménez, J. Skibsted, A. Palomo, Clay reactivity: Production of alkali activated cements, Applied Clay Science, 73 (2013) 11-16.

[32] C. Zhang, J. Xue, L. Fang, Mechanical perperties and microstructure of alkali-activated burned coal gangue cementitious material, J Chin Ceram Soc, 32 (2004) 1276-1280.

[33] Xinyuan Ke, Susan A. Bernal, Nan Ye, John L. Provis, J. Yang, One-Part Geopolymers Based on Thermally Treated Red Mud/NaOH Blends, J Am Ceram Soc, 98 (2015) 5-11.

[34] R.A. Antunes Boca Santa, A.M. Bernardin, H.G. Riella, N.C. Kuhnen, Geopolymer synthetized from bottom coal ash and calcined paper sludge, Journal of Cleaner Production, 57 (2013) 302-307.

[35] S. Kumar, R. Kumar, Mechanical activation of fly ash: Effect on reaction, structure and properties of resulting geopolymer, Ceramics International, 37 (2011) 533-541.

[36] J. Temuujin, R.P. Williams, A. van Riessen, Effect of mechanical activation of fly ash on the properties of geopolymer cured at ambient temperature, Journal of Materials Processing Technology, 209 (2009) 5276-5280.

[37] B. Świątkowski, E. Marek, Optimisation of pulverized coal combustion in O2/CO2/H2O modified atmosphere – Experimental and numerical study, Energy.

[38] A.J. Sarabèr, Co-combustion and its impact on fly ash quality; full-scale experiments, Fuel Processing Technology, 128 (2014) 68-82.

[39] R.S. Blissett, N.A. Rowson, A review of the multi-component utilisation of coal fly ash, Fuel, 97 (2012) 1-23.

[40] A.R. Ramsden, M. Shibaoka, Characterization and analysis of individual fly-ash particles from coal-fired power stations by a combination of optical microscopy, electron microscopy and quantitative electron microprobe analysis, Atmospheric Environment (1967), 16 (1982) 2191-2206.

[41] S. Sushil, V.S. Batra, Analysis of fly ash heavy metal content and disposal in three thermal power plants in India, Fuel, 85 (2006) 2676-2679.

[42] E. 450-1, Fly ash for concrete: Definition, specifications and conformity criteria, in, 2012.

[43] A. Fernández-Jiménez, A. Palomo, Composition and microstructure of alkali activated fly ash binder: Effect of the activator, Cement and Concrete Research, 35 (2005) 1984-1992.

[44] J.W. Phair, J.S.J. van Deventer, J.D. Smith, Effect of Al source and alkali activation on Pb and Cu immobilisation in fly-ash based “geopolymers”, Applied Geochemistry, 19 (2004) 423-434.

[45] D.L.Y. Kong, J.G. Sanjayan, K. Sagoe-Crentsil, Comparative performance of geopolymers made with metakaolin and fly ash after exposure to elevated temperatures, Cement and Concrete Research, 37 (2007) 1583-1589.

[46] K.L. Aughenbaugh, T. Williamson, M.C.G. Juenger, Critical evaluation of strength prediction methods for alkali-activated fly ash, Mater Struct, 48 (2015) 607-620.

[47] M. Komljenović, Z. Baščarević, V. Bradić, Mechanical and microstructural properties of alkali-activated fly ash geopolymers, Journal of Hazardous Materials, 181 (2010) 35-42.

[48] F. Pacheco-Torgal, J. Castro-Gomes, S. Jalali, Alkali-activated binders: A review. Part 2. About materials and binders manufacture, Construction and Building Materials, 22 (2008) 1315-1322.

[49] M. Criado, A. Palomo, A. Fernández-Jiménez, Alkali activation of fly ashes. Part 1: Effect of curing conditions on the carbonation of the reaction products, Fuel, 84 (2005) 2048-2054.

[50] J.L. Provis, J.S.J. van Deventer, Geopolymerisation kinetics. 1. In situ energy-dispersive X-ray diffractometry, Chemical Engineering Science, 62 (2007) 2309-2317.

[51] C. Shi, R.L. Day, A calorimetric study of early hydration of alkali-slag cements, Cement and Concrete Research, 25 (1995) 1333-1346.

[52] M. Criado, A. Fernández-Jiménez, A.G. de la Torre, M.A.G. Aranda, A. Palomo, An XRD study of the effect of the SiO2/Na2O ratio on the alkali activation of fly ash, Cement and Concrete Research, 37 (2007) 671-679.

[53] J. Davidovits, Mineral Polymers and the Methods of Making Them, in: U.S. Patent (Ed.) United States Patent, USA, 1982.

[54] P.D. Silva, K. Sagoe-Crenstil, V. Sirivivatnanon, Kinetics of geopolymerization: Role of Al2O3 and SiO2, Cement and Concrete Research, 37 (2007) 512-518.

[55] C.A. Rees, J.L. Provis, G.C. Lukey, J.S.J. van Deventer, In Situ ATR-FTIR Study of the Early Stages of Fly Ash Geopolymer Gel Formation, Langmuir, 23 (2007) 9076-9082.

[56] U. Rattanasak, P. Chindaprasirt, Influence of NaOH solution on the synthesis of fly ash geopolymer, Minerals Engineering, 22 (2009) 1073-1078.

[57] M.L. Granizo, M.T. Blanco, Alkaline activation of metakaolin – an isothermal conduction calorimetry study, J Therm Anal, 52 (1998) 957–965.

[58] M.S. Jansen, M.U. Christiansen, Effect of Water-solids ratio on the compressive strength and morphology of fly ash -waste glass geopolymer mortars, in: World of Coal Ash (WOCA) Conference, Nasvhille, TN, 2015.

[59] B. Mota, T. Matschei, K. Scrivener, The influence of sodium salts and gypsum on alite hydration, Cement and Concrete Research, 75 (2015) 53-65.

[60] C. Kuenzel, L.J. Vandeperre, S. Donatello, A.R. Boccaccini, C. Cheesman, Ambient Temperature Drying Shrinkage and Cracking in Metakaolin-Based Geopolymers, J Am Ceram Soc, 95 (2012).